JOURNAL OF CATALYSIS 142, 337–348 (1993)

Characterization of Pillared Montmorillonites with the Atomic Force Microscope (AFM)

M. L. OCCELLI,* B. DRAKE,† AND S. A. C. GOULD‡

*Zeolites and Clays Program, MST Laboratory, Georgia Tech Research Institute, Atlanta, Georgia 30332; †Imaging Services, Santa Barbara, California 93111; and ‡Claremont Colleges, Claremont, California 91711

Received March 17, 1992; revised January 19, 1993

An atomic force microscope (AFM) has been used to investigate the surface features of samples of Ca–bentonite from Texas and Na–bentonite from Wyoming that were pillared with alumina clusters. Atomic-scale-resolution images of the clay surface consist of hexagonal arrays of bright spots. The nearest-neighbor distance in the two parent clays was found to be consistently greater after pillaring in numerous images, suggesting that the bulky Al_{13} clusters stretched the clays' silicate layers. A number of images showed possible atomic resolution of oxygen atoms on the clay surface, suggesting that it can be possible to obtain resolution below the scale of the unit cell. Molecular-scale-resolution images of the cross-sectional area of extrudates formed using pillared Wyoming bentonite powder showed platelets about 9.0 Å apart, in agreement with X-ray diffraction (XRD) results. The presence of alumina debris or clusters on the silicate layer was not observed in any image examined, suggesting that the expended clay coking tendency during gas oil cracking can be attributed mainly to the strong Lewis-type acidity of the alumina pillars between the clay silicate layers.

INTRODUCTION

Smectites, when expanded with metal oxide clusters, can generate microporous solids with the necessary acidity and thermal stability required of catalysts used in conventional petrochemical processes such as hydrocracking. Today, the petroleum engineer is looking to these materials with renewed interest because certain pillared clays have been shown to have the hydrothermal stability typical of fluidized cracking catalysts (FCC) (*1–5*). In fact, thermal, as well as hydrothermal, stability in low-cost and readily available montmorillonite can be significantly enhanced by reacting a bentonite slurry in water with a solution of Chlorhydrol (from the Reheis Chemical Co.) that has been aged at high (180–200°C) temperatures in the presence of small amounts of lanthanides (Ce^{+4}, La^{+3}) ions (*3, 4*). Bentonite is the name of a rock containing more than 90% montmorillonite.

The drying method used to remove the fluid in an expanded clay after the pillaring reaction can determine the structure as well as the stability of a clay catalyst. Freeze-drying favors the formation of delaminated clays thermally stable to 500°C (*6*). In contrast, drying at critical conditions produces expanded montmorillonites and saponites with N_2 surface area in the 500–600 m^2/g range stable to 800°C (*7, 8*). Furthermore, the introduction of $SiO_2 \cdot TiO_2$ clusters in these materials generates macropores with acid-site density (and strength) lower than the one observed in clays pillared with Al_2O_3 or ZrO_2 clusters (*9, 10*). The moderate acidity, together with greater Bronsted/Lewis acid-site ratios, is believed responsible for the coke selectivity exhibited during gas oil cracking of a sample of saponite expanded with mixed $SiO_2 \cdot TiO_2$ clusters (*8*).

Modern spectroscopic techniques have provided useful information and many details concerning the properties of pillared montmorillonites. Mössbauer and X-ray photoelectron spectroscopy have indicated that iron impurities in a clay mineral can easily catalyze secondary cracking reactions and contribute to coke formation only when it is located inside the microporous

0021-9517/93 $5.00

structure, i.e., when it is found near the pillars (*11*). Transmission electron microscopy (TEM) and electron diffraction have shown the characteristic long-range stacking of silicate layers face-to-face in pillared montmorillonites (*12*). TEM has also been used to show that delaminated clays are instead characterized by short stacking of 10–15 layers. Face-to-edge and edge-to-edge orientation of these aggregates generate the macropores present in delaminated clays (*12*). Recently, TEM has been used to observe and study stresses that thermal treatments cause in pillared rectorites and to show that the exceptional stability of these clays can be attributed to the layer rigidity that the mica-like layers impart to the structure (*13*).

With the invention of the AFM by Binning *et al.* (*14*), which can generate atomic-scale images on some materials, geologists and chemists have a new tool to examine important samples. The AFM has already been used to study a few clay surfaces. Lindgreen *et al.* (*16*) investigated ultrafine particles of North Sea illite/smectite by AFM. Also, Hartman *et al.* (*15*) demonstrated the ability of the AFM to image molecular-scale features of montmorillonite and illite. This paper follows Hartman's work and examines the effects that pillaring with alumina clusters have on montmorillonite surfaces.

EXPERIMENTAL

Catalyst Preparation

A Ca–bentonite sample was obtained from the Southern Clay Products Company of Gonzales, Texas. A sample of Wyoming Na–bentonite was obtained from the American Colloidal Co.; these two samples have been described in detail elsewhere (*9*).

Ten grams of bentonite were slurried in 3 liter of DI water. An excess of an aluminum chlorhydroxide (ACH) solution (200 Meq Al/100 g Clay) was diluted to 500 cc and aged for 24 h at 50°C. The diluted chlorhydroxide was then slowly added to the clay slurry and allowed to react for 4 h at 60°C. The slurry was then filtered. The resulting cake was first washed with 1 liter DI water at 80°C and then dried in air at 100°C/10 h. A second 10-h drying step at 300°C was used to remove occluded water from the expanded structure. The pillared Tx-bentonite was crushed to a fine powder that was then pressed at 10,000 lbs/min into wafers 2.5 cm in diameter. The pillared Wy-bentonite was formed into extrudates and dried as indicated above. The wafers and the extrudates were then examined under the atomic force microscope in air.

Atomic Force Microscope (AFM)

The AFM used for these experiments (*17*) was a contact-mode microscope based on the optical lever cantilever detection design of Meyer and Amer (*18*) and Alexander *et al.* (*19*). The AFM works like a record player (see Fig. 1). An *xyz* piezoelectric

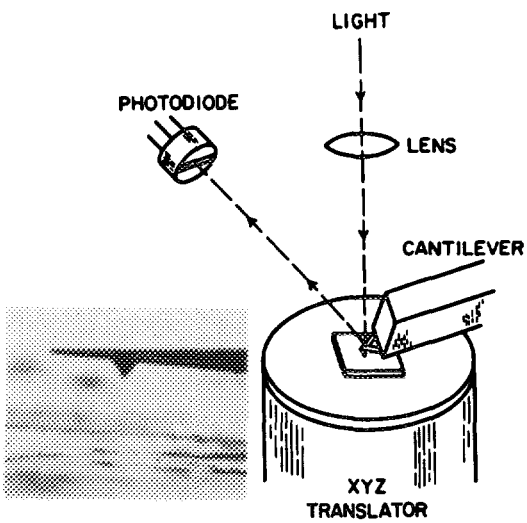

FIG. 1. Schematic diagram of the atomic force microscope (AFM) (*15*). Laser light is focused on the cantilever, which reflects it toward a photodiode. The photodiode senses the deflection of the cantilever by sensing the position of the reflected beam. In operation, a feedback loop keeps the position of the reflected beam, and hence the force on the sample, constant. This was accomplished by moving the sample up and down with the *z*-axis of the *xyz* translater as the sample was scanned underneath it with the *x*- and the *y*-axes (*28*). The insert shows a photomicrograph of the silicon nitride cantilever used (Greg Kelderman, UCSB).

translator raster scans a sample below the stylus of the cantilever. The vertical deflection (z-direction) of the cantilever, as the stylus moves over the topography of the surface, is measured by reflecting a laser beam off the end of the cantilever and measuring the location of the reflected laser light with a two-segment photodiode. A digital electronic feedback loop keeps the deflection of the cantilever, and hence the force of the stylus on the surface, constant. This is accomplished by moving the sample up and down in the z-direction of the xyz translator as the sample is scanned in the x- and y-directions. The images contain either 200-by-200 or 400-by-400 data points, and nearly all images in this study were acquired within a few seconds. The Si_3N_4 cantilevers (with integral tips) used for imaging were 120 μm in length and possessed a spring constant of approximately 0.6 N/m. In this study, the force applied for these images ranged from 10–100 nN, and more than 100 images were examined.

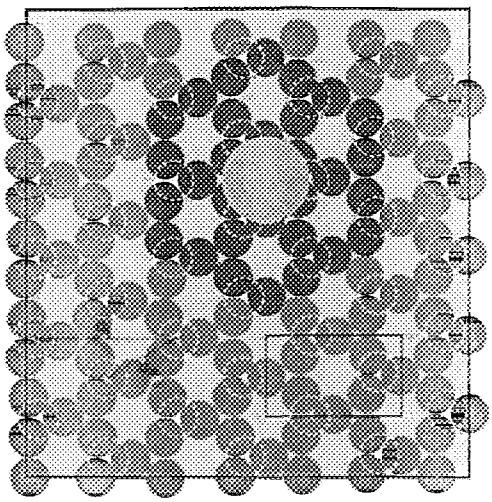

FIG. 2. Hexagonal array of oxygen ions on the basal plane of a 2 : 1 clay mineral. The three basal oxygens of a SiO_4 (shown as small gray circles) form hexagonal oxygen rings with 2.6-Å opening. The fourth oxygen of a SiO_4 unit points toward the clay octahedral layer. Possible location and area occupied by the Al_{13} ion has been highlighted. A unit cell (5.4 × 11.0 Å) and the lateral dimensions, d_1 and d_2, are shown by solid lines (*27*).

RESULTS AND DISCUSSIONS

Montmorillonite is a 2:1 layered clay consisting of two layers of SiO_4 tetrahedra sandwiching a layer of Al atoms in octahedral coordination (*23*). The SiO_4 units are joined together by sharing their three basal oxygens to form a hexagonal array of oxygen rings, as represented in Fig. 2 (*27*). The fourth oxygen (the apical oxygen) points, in a direction normal to the plane, into the layered structure to connect the SiO_4 layer with the octahedral sheet (*23, 27*).

Isomorphous substitution of Al with divalent ions (and to a lesser extent, of Si with Al) gives to the clay silicate layers a negative charge compensated mainly by Na or Ca ions (*23*). By ion exchanging Ca^{+2} ions (in the Tx-bentonite) or Na^+ ions (in the Wy-bentonite) with a chlorhydroxide solution containing $[Al_{13}O_4(OH)_{24}(H_2O_{12}]^{+7}$ ions, expanded clay minerals with N_2 surface area of 314 and 298 m^2/g were obtained that retained their microporous structure even when calcined in air at 500°C/10 h (*9*).

A schematic representation of the exchange reaction and of the resulting pillared montmorillonite structure is given in Fig. 3. As expected, the exchange reaction with the bulky Al_{13} ions caused the $d(001)$ reflection

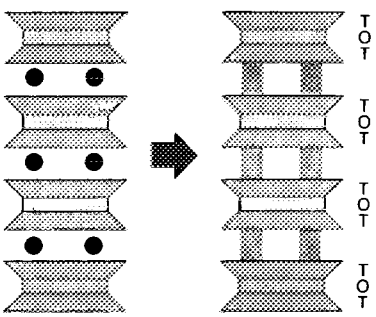

FIG. 3. Schematic representation of the pillaring reaction. The T–O–T three-layer sequence (T = tetrahedral, O = octahedral) in montmorillonite is represented by trapezoids and rectangles. Exchange of charge-compensating cations (solid circles) with Al_{13} ions expands the silicate layers. On calcination, the bulky oxycations form pillars that expose the interlamellar space to sorption and catalysis.

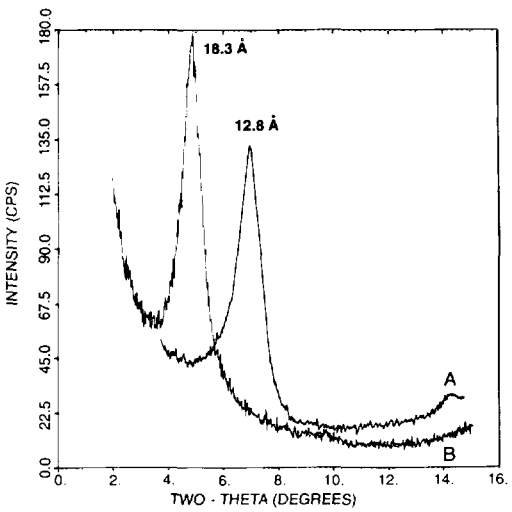

FIG. 4. X-ray diffractograms of a sample of Tx-bentonite (A) before and (B) after pillaring with Chlorhydrol and calcination at 400°C/10 h in air.

of the two clay samples to shift to lower diffraction angles (see Figs. 4 and 5). A change of the clay basal spacing from 12.8 to 18.3 Å corresponds to an expansion of the clay silicate layers of about 8.7 Å (Fig. 4). On dehydroxylation (at 500°C/10 h, air), the Al_{13} ions shrank in size and the pore height of the microspace generated by pillaring decreased to 8.0 from 8.7 Å, a result

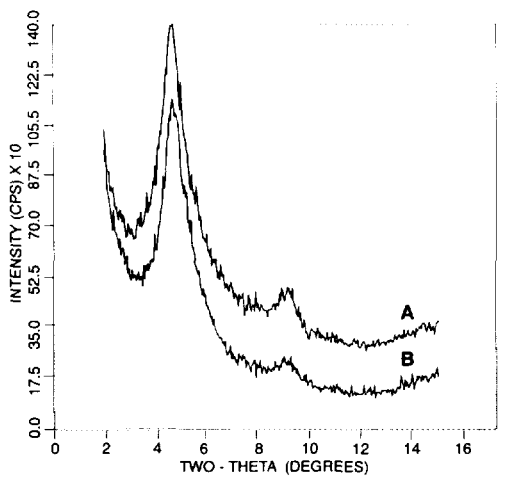

FIG. 5. X-ray diffractograms of a sample of Wy-bentonite pillared with Chlorhydrol (A) before and (B) after formation of extrudates 0.16 cm in diameter.

in agreement with the Al_{13}-ion dimension of about 8.0 Å (*26*).

The pore width of the microporous structure depends on the Al_{13} ions' distribution on the clay silicate layers. Sorption and diffusion measurements (*24, 25*) have indicated that although the charge density distribution in montmorillonites may not be homogeneous, a fairly uniform distribution of Al_{13} clusters is present. In fact, pillared bentonites can sorb similar volumes (0.8–1.0 cc/g) of C_5–C_{10} *n*-paraffins (*23*) and can easily sorb 1,3,5-trimethylbenzene (mesylene). When (Fig. 2) the cavity of a hexagonal ring of oxygens and the oxygen–oxygen distance are 2.6 and 2.8 Å, respectively (*15*), the nearest distance between the three basal oxygens (of adjacent SiO_4 units), d_c, is about 5.4 Å and the lateral distance, d_l, between these units is about 11.0 Å. In Fig. 2, possible Al_{13} pillar next-neighbor distances are 14.58, 15.42, or 16.72 Å, implying pore widths of 6.58, 7.42, or 8.72 Å that are consistent with sorption data. Residual monovalent (or divalent) cations could be present together with the Al_{13} ions to fully charge compensate the clay silicate layers. The AFM could image the clay surface structure and provide detail with molecular-scale resolution of the sorption of polyoxocation effects in pillared clay catalysts.

AFM images of Tx- and Wy-bentonite surfaces before and after pillaring are shown in Figs. 6–9, respectively. Large-scale-resolution images of these clay samples are shown in Figs. 6A–8A; the same Si_3N_4 tip was used to generate images for a given set of samples. At the atomic scale, images of Ca- or Na-montmorillonites (before and after pillaring) consist of a hexagonal array of bright spots that gave the image a kernel-like appearance (see Figs. 6B–9B). Irregularities in the distribution of these bright spots were not uncommon. The observed lateral distance, d_l, between bright spots is in the 8.5–10 Å range for all samples (see Table 1). During the numerous scanning sessions, over 100 images were

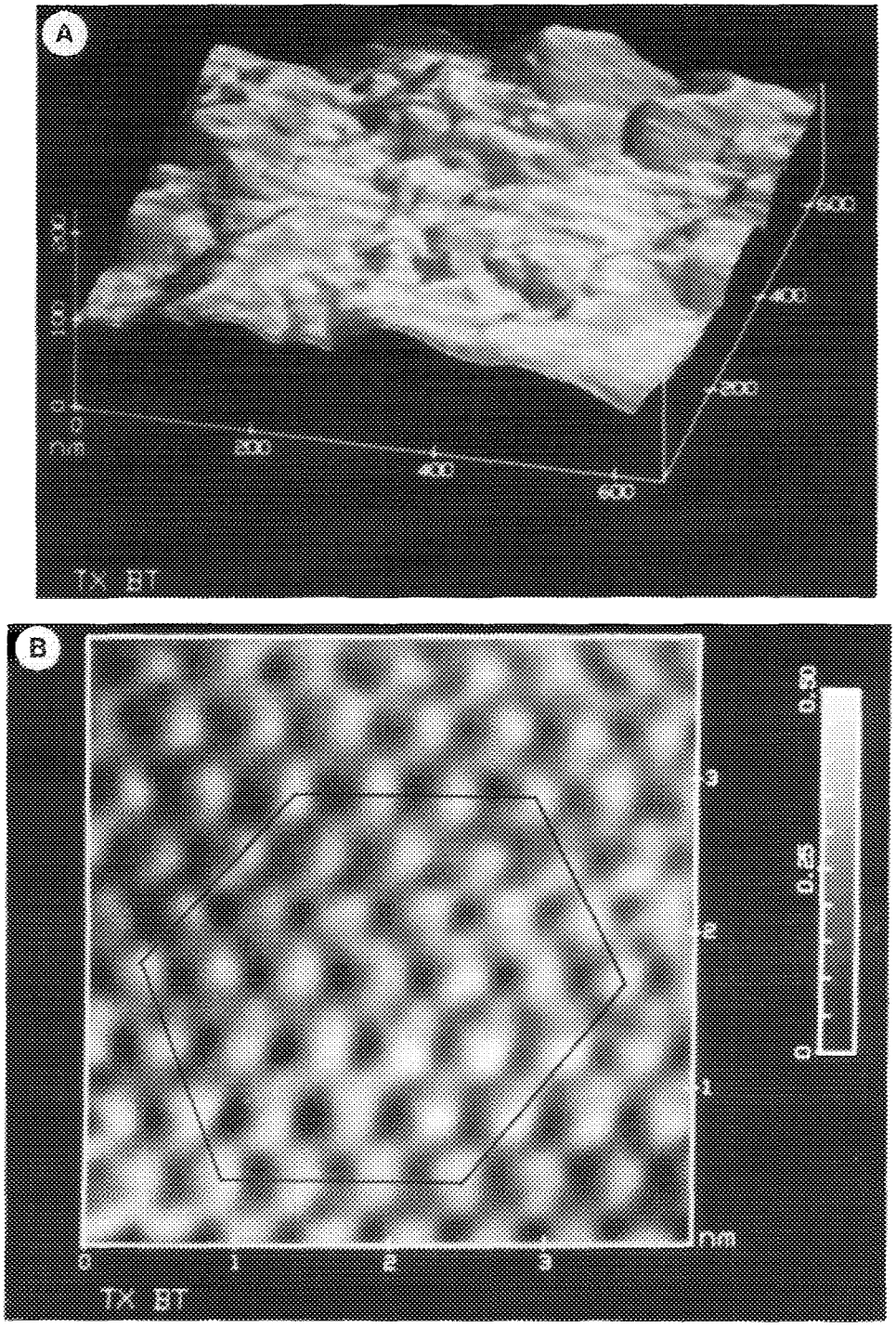

FIG. 6. (A) Large-scale AFM image of a TX-bentonite surface. (B) Atomic-resolution image of the clay tetrahedral layer (top view). The insert shows the hexagonal arrangement of bright spots on the basal plane.

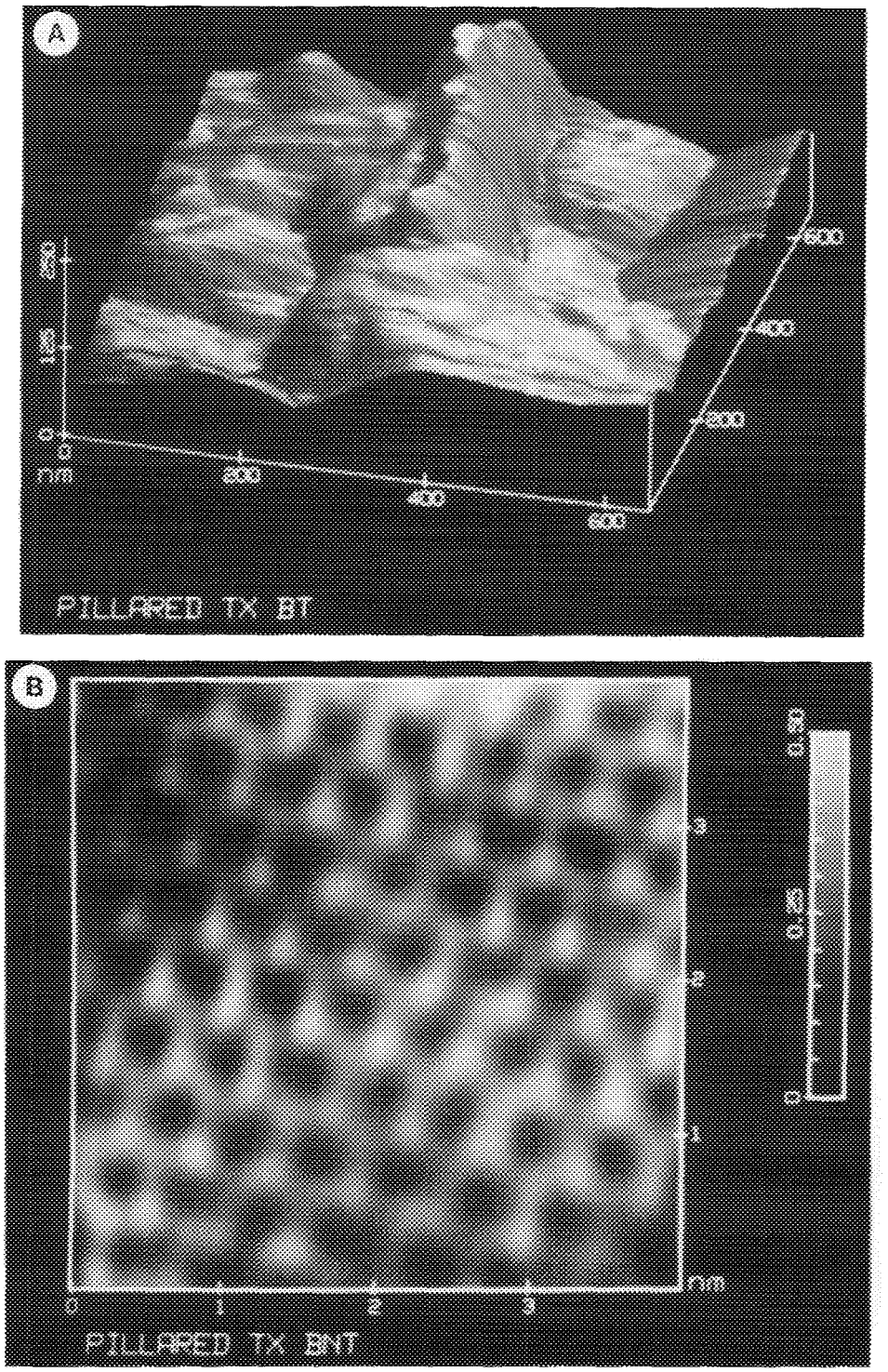

FIG. 7. (A) Large-scale AFM image of a pillared Tx-bentonite surface. (B) Atomic-resolution image of the clay tetrahedral layer (top view). (C) The white spots 2.7 Å apart (indicated by arrows) in a hexagonal arrangement are believed to represent oxygen anions.

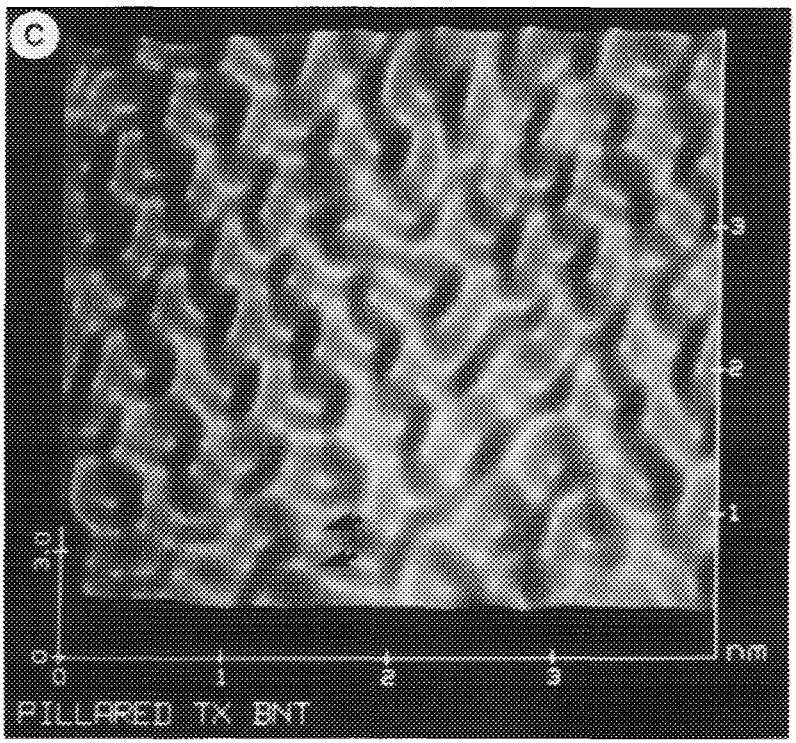

FIG. 7—*Continued*

saved for analysis. To obtain the most accurate results, surface parameters were measured when the images possessed the least amount of thermal drift. Extreme thermal drift can be detected during scanning by rotating the image by 90° and noting changes in the dimension of the unit cell. Less extreme thermal drift is apparent when analyzing the two-dimensional power spectrum of the image because of the sample symmetry. In general, it was found that images possessing the least thermal drift were the ones taken from the end of an imaging session when the microscope and the sample reached complete thermal equilibrium. The image processing used in Figs. 6B–9B consisted of a back-plane subtraction to level the image, and a mild low-pass filter to eliminate spurious noises beyond the resolution of the microscope. In general, image processing has been minimal.

The average nearest-neighbor distance (the spot-to-spot distance, d_c) before and after pillaring with Al_3 ions (including standard deviation) is indicated in Table 1. A spectrum of values for d_c and d_1 was measured. However, the majority of the measurements were near the average reported, as demonstrated by the low values for the standard deviation shown in Table 1. Although the differences between the pillared and the parent samples were not large (which was not unexpected because exten-

TABLE 1

Molecular Parameters for the Surface of Several Montmorillonites before and after Pillaring with Al_{13} Ions

	d_c (Å)	s.d.	d_1 (Å)	s.d.	Images
Tx-bentonite	5.15 ± 0.5	0.25	8.9 ± 0.9	0.35	10
ACH-(Tx-bentonite)	5.45 ± 0.5	0.20	9.4 ± 0.9	0.35	12
Wy-bentonite	4.70 ± 0.5	0.40	8.1 ± 0.9	0.70	8
ACH-(Wy-bentonite)	5.37 ± 0.5	0.41	9.3 ± 0.9	0.70	6

Note. The errors shown indicate upper and lower limits observed for d_1 and d_c during the examination of 36 images.

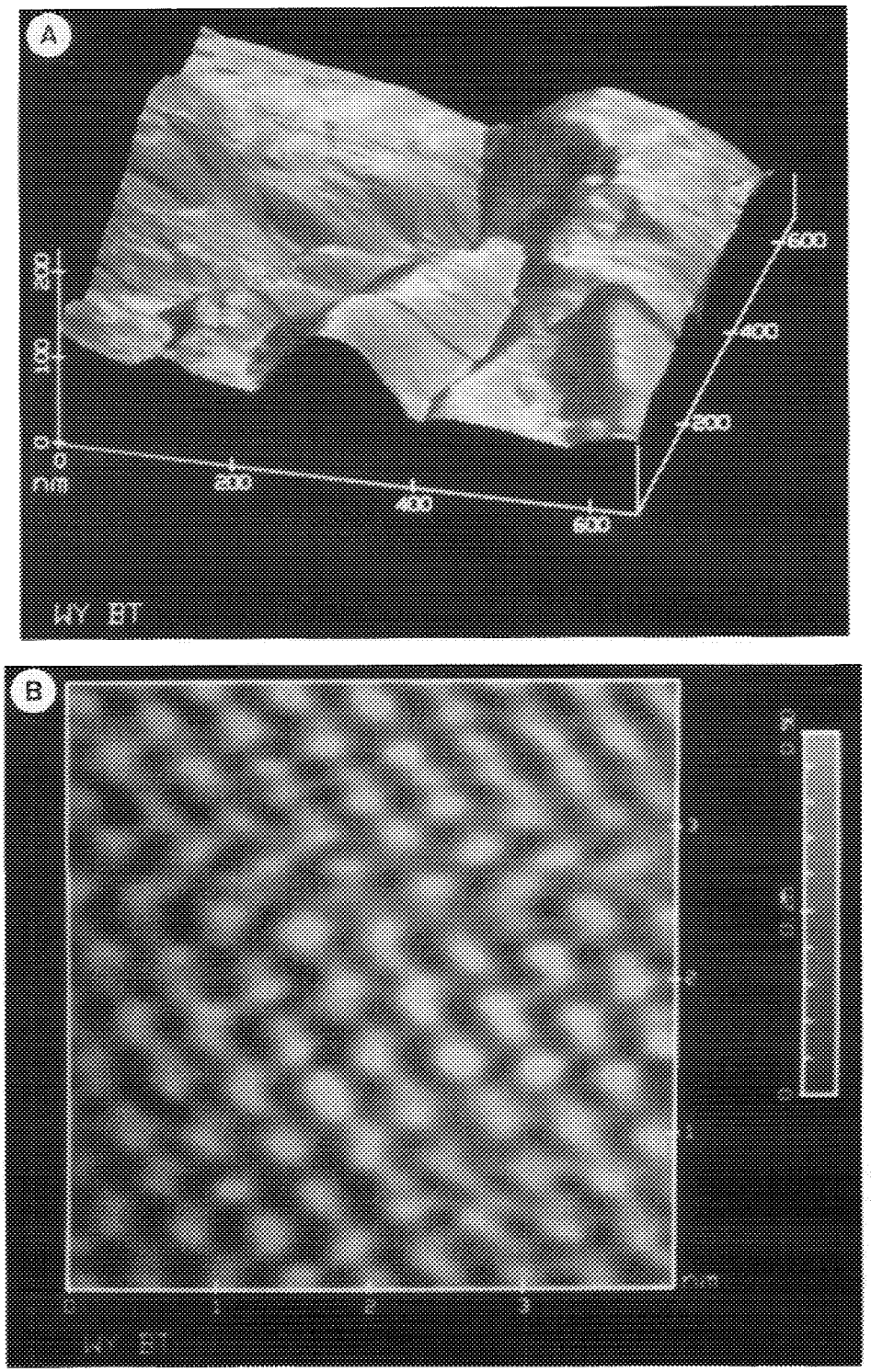

FIG. 8. (A) Large-scale AFM image of a Wy-bentonite surface. (B) Atomic-resolution image of the clay tetrahedral layer.

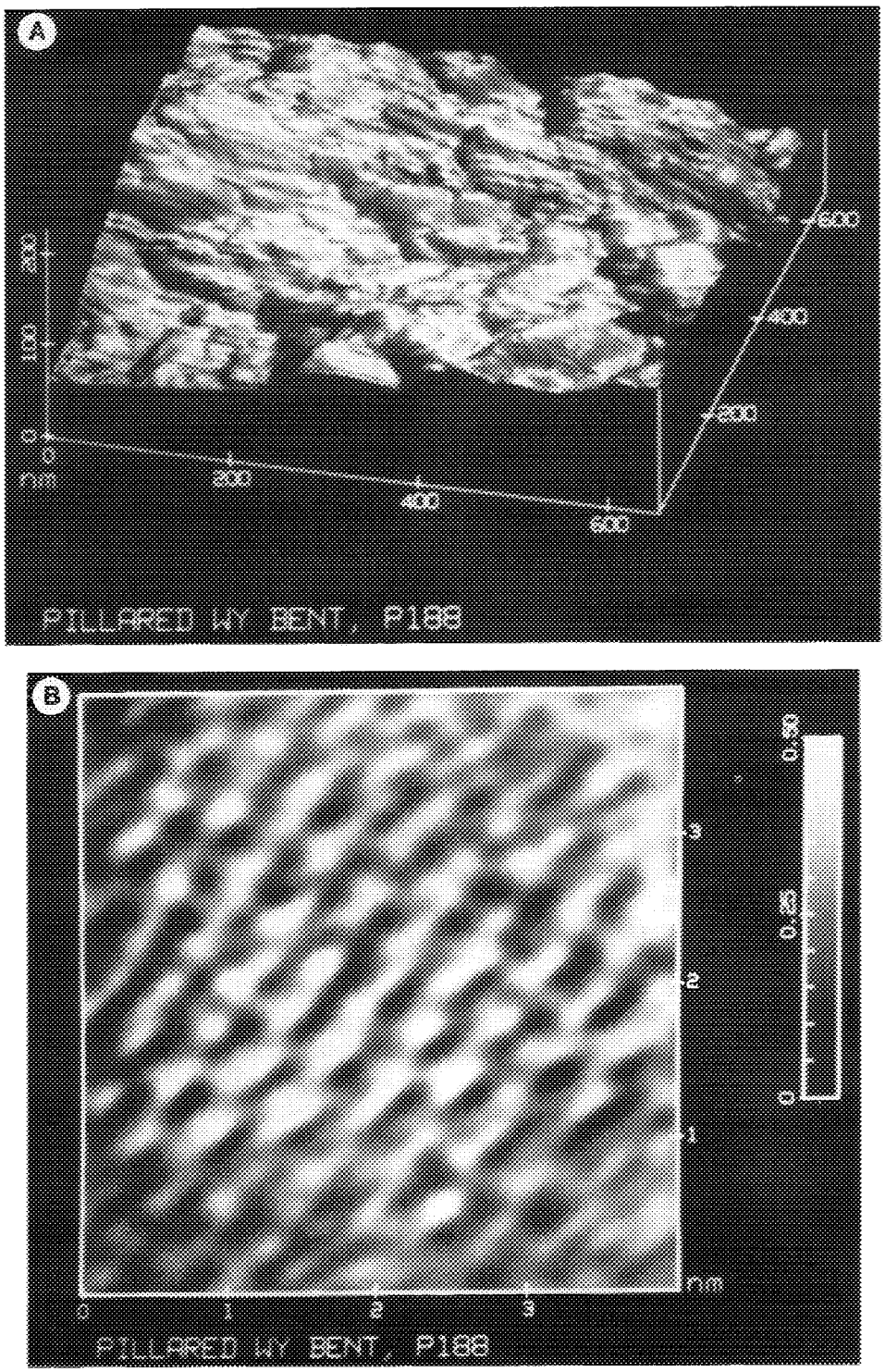

FIG. 9. (A) Large-scale AFM image of a pillared Wy-bentonite surface. (B) Atomic-resolution image of the clay tetrahedral layer.

sive bond breakage did not occur during the pillaring reaction), it was consistently observed that pillared montmorillonites possessed larger nearest-neighbor distances than the parent materials. The similarity between these molecular parameters with those (11.0 and 5.4 Å) measured in Fig. 2 using simple geometric argument suggests that in Figs. 6–9 the bright spots represent the three basal oxygens of a SiO_4 unit. Also, the dark spots represent holes in the center of hexagonal rings of oxygen atoms (see Fig. 2). Hartman *et al.* (*15*) have instead proposed that the bright spots represent hexagonal rings of oxygen anions.

The pillaring reactions seem to increase the center-to-center distance between bright spots (Table 1). We surmise that by replacing the parent-clay charge-compensating cations with Al_{13} ions in the interlamellar space, a stretching of the SiO_4 layers occurs. In the upper left-hand corner of Fig. 7B, detail below the unit cell dimensions can be resolved. It is believed that the small white spots (Fig. 7C) spaced at 2.7 ± 0.3 Å apart are individual oxygen anions in a hexagonal arrangement. Figure 7C has been shaded to better display the individual oxygen anions. Therefore, it is possible to obtain resolution below the scale of the unit cell with the AFM.

In all the images obtained, the hexagonal holes appeared to be empty. Because similar observations have been made for calcined (100–500°C, in air) samples, it is doubtful that the AFM scanning tip could have displaced surface cations from the hexagonal holes. Thus, charge-compensating cations (Na, Ca, or Al_{13} ions) are preferentially located into the montmorillonite interlamellar space.

The pillared Wy-bentonite powder was formed into extrudates and their cross-sectional area exposed to the AFM (i.e., across the planes) in the hope of observing the alumina pillars sandwiched between the clay silicate layers. The forming process caused only a small decrease in N_2 surface area (to 280 from 298 m^2/g); the XRD diffractograms in Fig. 5 indicate that the clay 001 reflection remained unchanged near 18.1 Å, suggesting that the forming of the clay powders into extrudates has little affect on the pillard structure. The AFM images in Fig. 10 shows the orientation face-to-face of the clay silicate layers and their expansion resulting from the presence of Al_2O_3 clusters. Although there is a distribution of expanded layers, the measured basal spacing in Figure 10 is 9.0 ± 1.0 Å, a result in agreement with the one (8.5 Å) obtained by XRD (see Fig. 5). Direct observation of Al_2O_3 clusters (pillars) between the layers could not be made.

Examination of over 100 images has revealed a constant relationship between the clay surface atomic parameters (d_1 and d_c) observed with the AFM and the geometrical parameters of the montmorillonite basal plane shown in Fig. 2. Thus, it is believed that montmorillonites pillared with Al_{13} clusters do not contain on their surface alumina debris (or pillars) that could enhance the coking tendency of these clay catalysts (*9*). Similar observations have been made while inspecting pillared hectorite, saponite, and rectorite catalysts (*29*). These results lend support to previous studies reporting that the high carbon generation of expanded clays during gas oil cracking (*9*, *11*) can be attributed mainly to the strong Lewis-type acidity of the alumina pillars placed between the clay silicate layers. The strong Lewis acidity generated by the pillaring reaction is what favors the retention of aromatics, and therefore coke formation (*11*), in these catalysts.

SUMMARY

The atomic force microscope can generate images that provide atomic-scale details of the basal plane of clays and clay catalysts with resolution below the scale of the unit cell. It has been observed that the pillaring reaction with Al_{13} ions stretches the montmorillonite SiO_4 layers and that alumina clusters or debris are not present on the clay surface. Thus, surface alumina im-

purities cannot be responsible for the ease with which these clay catalysts deactivate due to coke formation. Because all measurements were performed in air, the AFM allowed the characterization of solid surfaces without the possibility of altering their molecular features. Thus, the AFM could be particularly useful in studying commercially important material such as FCC and in hydrotreating catalyst surfaces.

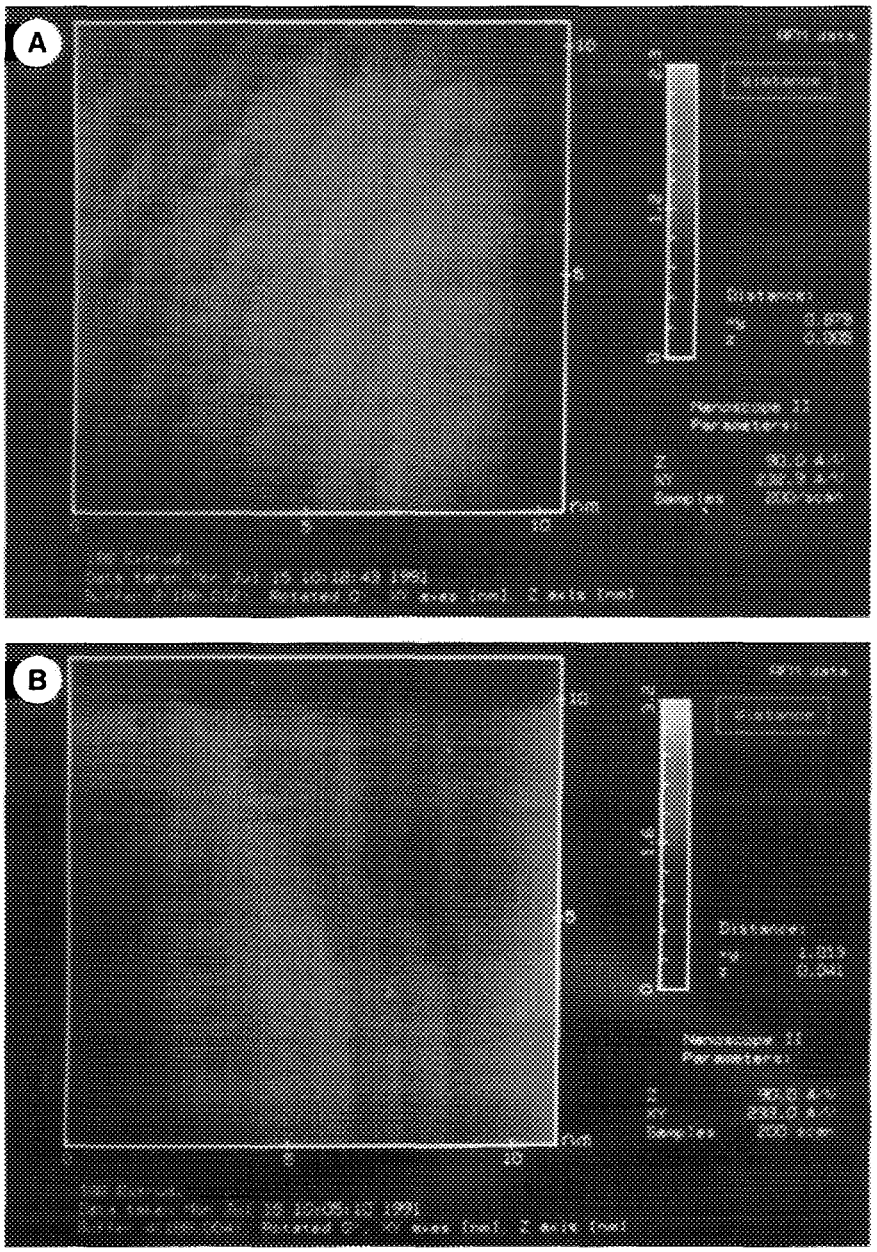

FIG. 10. (A, B) AFM images of the cross-sectional area of a 0.16 cm extrudate formed using a pillared Wy-bentonite. The distance measured using the photomicrograph scale is well in agreement with XRD results. However, alumina pillars could not be observed.

ACKNOWLEDGMENTS

The authors are particularly grateful to Professors P. K. Hansma and M. Wilson (UCSB) for help and encouragement received during the initial stage of this study. Special thanks are due to Mr. M. Bell (Unocal) for providing XRD data.

REFERENCES

1. Guan, J., Min, E., Yu, Z., Zheng, H., and Liang, Y. *in* "Proceedings, China–Japan–USA Symposium on Heterogenous Catalysts Related to Energy Problems," paper BO2C, p. 7 (1982).
2. Guan, J., Min, E., and Yu, Z., U.S. Patent 4,757,040 (1986).
3. McCauley, J. R., U.S. Patent 4,952,544 (1990).
4. Sterte, J., *in* "Preparation of Catalysts V" (G. Poncelet, P. A. Jacobs, P. Grange, and B. Delmond, Eds.), p. 301. Elsevier, Amsterdam, 1991.
5. Occelli, M. L., *in* "Preparation of Catalysts V" (G. Poncelet, P. A. Jacobs, P. Grange, and B. Delmond, Eds.), p. 287. Elsevier, Amsterdam, 1991.
6. Pinnavaia, T. J., Izon, M. S., Landau, S. D., and Raythathe, R. H., *J. Mol. Catal.* **27,** 195 (1984).
7. Takahama, K., Yokoyama, M., Hirao, S., Yamanaka, S., and Hattori, M., *J. Mat. Sci,* in press.
8. Occelli, M. L., Takahama, K., Yokoyama, M., and Hirao, S., *in* "Proceedings International Symposium on Zeolites and Pillared Clays Synthesis, New York, August 24, 1991," submitted.
9. Occelli, M. L., *in* "Keynotes in Energy Related Catalysis" (S. Kaliaguine, Ed.), p. 101. Elsevier, Amsterdam, 1988.
10. Parry, E. P., *J. Catal.* **2,** 371 (1963).
11. Occelli, M. L., Stencel, J. M., and Suib, S. L., *J. Mol. Catal.* **64,** 221 (1991).
12. Occelli, M. L., Lynch, D. J., and Sanders, J. V., *J. Catal.* **197,** 557 (1987).
13. Dominguez, J. M., and Occelli, M. L., *in* "Proceedings, International Symposium on Zeolites and Pillared Clays Synthesis, New York, August 24, 1991," in press.
14. Binning, G., Quate, C. F., and Gerber, C., *Phys. Rev. Lett.* **56,** 430 (1986).
15. Hartman, H., Sposito, G., Yang, A., Manne, S., Gould, S. A. C., and Hansma, P. K., *Clays Clay Miner.* **38,** 4, 337 (1990).
16. Lindgreen, H., Garnaes, J., Hansen, P. L., Besenbacher, F., Laegsgaard, E., Steinsgaard, Gould, S. A. C., and Hansma, P. K., *Am. Miner.* **76,** 1218 (1991).
17. Digital Instruments, Inc., 6870 Cortona Dr., Goleta, CA 93117.
18. Meyer, G., and Amer, N. M., *Appl. Phys. Lett.* **53,** 1095 (1988).
19. Alexander, *et al., J. Appl. Phys.* **65,** 164–167.
20. Ruger, D., and Hansma, P. K., *Phys. Today* **October,** 23 (1990).
21. Gould *et al., J. Vac. Sci. Technol. A* **8,** 369 (1990).
22. Albrecht, T. R., and Quate, C. F., *J. Vac. Sci. Technol. A* **6,** 271 (1988).
23. Grim, R. E., "Clay Mineralogy." McGraw–Hill, New York, 1968.
24. Occelli, M. L., Innes, R. A., Hwu, F. S. S., and Hightower, J. W., *Appl. Catal.* **14,** 69 (1985).
25. Occelli, M. L., Parulekar, V. N., and Hightower, J. W., *in* "Proceedings, 8th International Congress on Catalysis, Berlin, 1984," Part IV, p. 725. Dechema, Frankfurt-am-Main, 1984.
26. Johansson, G., *Acta Chem. Scand.* **14,** 769 (1960).
27. Bailey, S. W., *in* "Review in Mineralogy" (S. W. Bailey, Ed., Vol. 13. The Mineralogical Society of America, Washington, DC, 1984.
28. Drake, B., *et al., Science* **243,** 1586 (1989).
29. Occelli, M. L., Gould, S. A. C., and Drake, B., in preparation.